Statistical investigations of the flow-aligned component of IMF impact on current sheet structure in Martian magnetotail: MAVEN observations

Yuanzheng Wen[1, 2], Zhaojin Rong[2, 3], Hans Nilsson[4], Chi Zhang[2, 3], Mats Holmstrom[4], Dan Tao[1], Guangxue Wang[1], Yiteng Zhang[5], Jasper Halekas[6], Jared Espley[7]

[1]School of Geophysics, Chengdu University of Technology, Chengdu, China.

[2]Key Laboratory of Earth and Planetary Physics, Institute of Geology and Geophysics, Chinese Academy of Sciences, Beijing, China.

[3]School of Earth and Planetary Sciences, University of Chinese Academy of Sciences, Beijing, China.

[4]Swedish Institute of Space Physics, Kiruna, Sweden.

[5]National Space Science Center, Chinese Academy of Sciences, Beijing, China.

[6]Department of Physics and Astronomy, University of Iowa, Iowa City, USA.

[7]NASA Goddard Space Flight Center, Greenbelt, USA.

Corresponding author: Zhaojin Rong (rongzhaojin@mail.iggcas.ac.cn)

Key Points:

- There is a systematic Y (i.e., dawn-dusk) asymmetry in the location of the Martian magnetotail current sheet in the modified MSE coordinates
- The asymmetry is controlled by the flow-aligned component of IMF, shifting to the dawn (-Y) during the tailward IMF conditions and to the dusk (+Y) during the sunward IMF conditions
- The shift found in this study is mostly dominated by the IMF, with minor contributions from the crustal magnetic fields and solar EUV intensity.

Abstract

In this study, we investigated the role of IMF orientation at controlling the location and structure of the current sheet in Martian magnetotail. Here based on carefully selected cases as well as statistical studies by using the magnetic field data of MAVEN MAG from October 2014 to February 2020, our study shows the IMF orientation can systematically influence the magnetotail current sheet structure of Mars. It is found that significantly tailward IMF conditions result in a Venus-like magnetotail configuration with the current sheet shifted to the -Y (dawnside) direction. Sunward IMF conditions result in a tail configuration with the current sheet shifted to the +Y (duskside) direction. The lobes follow this pattern, with the current sheet shifting away from the larger lobe. However, the current sheet did not show significant displacement under cross-flow dominant IMF conditions. Moreover, crustal magnetic fields and other factors can also influence the current sheet structure, but the IMF orientation is still the dominant controlling factor from our study. Our results demonstrates that the flow-aligned component of the IMF can influence and systematically control the current sheet structure in Martian magnetotail.

Plain Language Summary

Mars, which does not have an intrinsic magnetic field, has formed an induced magnetic environment from the draping of the interplanetary magnetic field (IMF) from the Sun. It folds around Mars, forming two “lobes” of magnetic field behind the planet with a current sheet of electrified gas (plasma) behind it. The current sheet is not always directly behind the planet but rather shifted toward the dawn or dusk direction. It is shown in our study that one factor that can control the location of the current sheet is the flow-aligned component of the IMF (B_X). The current sheet is shifted toward dawn (+Y) under sunward IMF condition and shifted dusk (-Y) under tailward IMF condition, while the current sheet shows little displacement under cross-flow IMF condition.

1 Introduction

Mars, which is like Venus, lacks a strong internal dipole magnetic field, so the solar wind and interplanetary magnetic field impacts directly on Mars’s ionosphere and atmosphere (*Nagy et al.*, [2004]; *Bertucci et al.*, [2011]). The interaction induces ionospheric electric currents in the

ionosphere, which causes the IMF to pileup and drape over the planet. This results in the formation of two magnetic lobes behind the planet, a tail current sheet (CS) is between the two lobe regions with antiparallel filed lines (*Dubinin and Franze* [2015]).

An earlier study by *McComas et al*. [1986], found an interesting feature of the magnetotail of Venus using Pioneer Venus Orbiter (PVO) data from the distant tail, which is that its location to the planet exhibits a dawn-to-dusk asymmetry. In the statistical study, it is found that the average location of the CS center is shifted toward the $+B_X$ by 0.5 R_V. The average magnetic field angle in the lobe of $-B_X$ hemisphere is -78.4° and 73.4° in the lobe of $+B_X$ hemisphere. The lobe transverse width of the $-B_X$ hemisphere and the $+B_X$ hemisphere are estimated to be 2.1 R_V. and 1.6 R_V., respectively. The amplitude of X component of magnetic field in the lobe of $-B_X$ hemisphere is found larger than that in the $+B_X$ hemisphere, it is suggested that the flow-aligned component of the IMF influences the magnetic field configuration of Venusian magnetotail. This shift was confirmed by magnetohydrodynamics (MHD) calculations of the Venus space environment by *Ma et al.* [2013]. However, by using the magnetic field data of Venus Express (VEX) from April 2006 to December 2014, along with carefully selected cases and the statistical studies, *Rong et al*. [2016] showed that the exact structure of the near-Venus magnetotail asymmetry is actually insensitive to the flow-aligned component of the IMF. The IMF B_X cannot significantly impact the magnetic field structure over current sheet. From their study, the true reason for the shift still seems to be an open issue.

Similarly, the shift has also been observed at Mars and Titan. Previous simulations by *Simon et al.* [2009] showed that the flow-aligned component of the IMF can displace the current sheet and cause the asymmetric structure in the magnetotail of Titan. Moreover, by checking the magnetic field data of Cassini for 85 flybys of Titan, *Simon et al.* [2013] found a consistent correlation between the shift of the current sheet and corotation flow component of the background magnetic field. By using the data from Mars Global Surveyor (MGS), *Halekas et al.* [2006] found many current sheet crossings in upper ionospheric magnetic data at 2 A.M. local time, implying a systematic -Y shift in the magnetotail current sheet. In contrast, *DiBraccio et al*. [2015] showed observations of a satellite pass in the near-Mars tail, demonstrating a shift to the +Y direction for the magnetic field reversal (the location of the current sheet). Moreover, *Romanelli et al.* [2015] used magnetometer data from the MGS and checked the distributions of data points in Martian

magnetotail for different polarities of IMF B_X and found a correlation between the IMF and its lobes, their results seem to align with *McComas et al*. [1986]. However, their analysis technique is similar to *McComas et al.* [1986] for Venus. Moreover, in their study there is a lack of the simultaneous measurement for the upstream solar wind and IMF conditions, which are always changing during the time spacecraft spends inside the induced magnetosphere. Thus, we cannot conclude that whether the IMF really influences the current sheet structure in magnetotail of Mars since previous study by *Rong et al.* [2016] suggested IMF B_X cannot influence the current sheet structure in near-Venus magnetotail. Besides, *Romanelli et al.* [2015] discarded all MAG measurements occurring inside the MPB for which the X_{MSO} coordinate is higher than -1.5 R_M to filter out the potential effects of crustal magnetic fields, while several studies have found systematic influences of the crustal magnetic field locations on magnetotail configurations [*Ma et al.*, 2002*; Harnett and Winglee*, 2005*; Fang et al.*, 2010, 2015*; Dong et al.*, 2015].

In this study we investigated the influence of the IMF orientation on the morphology of the current sheet in a much more accurate way based on carefully selected cases along with statistical studies, using MAVEN data from October 2014 to February 2020. Considering the varying upstream solar wind condition, we restricted the study to cases where the upstream IMF variations are as small as possible. Besides, we also considered the effects from the crustal magnetic fields and other factors that may influence the magnetotail configurations, and compared the contributions of these factors. The study is constructed as follows: the instruments and data set applied to this study are briefly introduced in section 2. The analysis technique used to quantitively evaluate the current sheet structure displacement is presented in section 3. Results from analysis based on selected cases are shown in section 4, while we showed the results from the statistical studies in section 5. In section 6, we summarized our discussions and conclusions.

2 Instrumentation and Data Set

The MAVEN spacecraft was inserted into orbit about Mars on 21 September 2014 and, after a brief commissioning phase, began its primary science investigation on 16 November 2014. MAVEN's 4.5 h elliptical orbit reaches periapsis and apoapsis altitudes of ~150 km and ~6200 km, respectively. The 74° inclination orbit provides global coverage of the Martian space environment, sampling a full range of latitudes and local times over the course of its orbital evolution. [*DiBraccio et al*., 2017]

In this study, the magnetic field, ion and electron data from MAVEN. [*Jakosky et al*., 2015] were adopted to identify the current sheet crossing cases. The magnetometer (MAG) [*Connerney et al.*, 2015] provides vector magnetic field data at a maximum sampling rate of 32 vectors per second. The Solar Wind Ion Analyzer (SWIA) [*Halekas et al*., 2013] and Suprathermal and Thermal Ion Composition (STATIC) [*McFadden et al*., 2015] instruments measure the flux, energy, and distributions of ions throughout the Martian space environment at cadences up to 4s. The Solar Wind Electron Analyzer (SWEA) [*D. L. Mitchell et al.*, 2015] provides electron distributions as often as once every 2s. MAVEN observations are reported in Mars solar orbital (MSO) coordinates, unless otherwise stated: X_{MSO} is directed from the center of the planet toward the Sun, Z_{MSO} is normal to Mars' orbital plane, and Y_{MSO} completes the right-handed system.

3 Analysis Technique

3.1 The Normal of the Current Sheet

The knowledge of the normal to the Current Sheet (CS) should be required to study the current sheet structure in the Martian magnetotail. The minimum variance analysis (MVA) [*Sonnerup and Scheible*., 1998] is applied to the MAG data over individual current sheet encounter to determine the CS normal direction ($\hat{n}$). Considering the boundary conditions $B_{1n} = B_{2n}$ at the magnetic discontinuity (because of $\nabla \cdot B = 0$), where B_{1n} and B_{2n} are the normal components of magnetic fields at both sides of discontinuity, the normal direction $\hat{\mathbf{n}}$ can be determined by minimization of

$$\sigma^2 = \frac{1}{N}\sum_{i=1}^{N} |(\mathbf{B}_i - \langle \mathbf{B} \rangle) \cdot \hat{\mathbf{n}}|^2 \quad (1)$$

Where $\langle \mathbf{B} \rangle = \frac{1}{N}\sum_{i=1}^{N} \mathbf{B}_i$ and i=1, 2, 3…. N. N is the number of data points. With the MVA, the local Cartesian coordinates, $\{\boldsymbol{X_1}, \boldsymbol{X_2}, \boldsymbol{X_3}\}$, for a CS can be set up. The $\boldsymbol{X_1}$, $\boldsymbol{X_2}$, $\boldsymbol{X_3}$ are orthogonal eigenvectors ($\boldsymbol{X_3} = \boldsymbol{X_1} \times \boldsymbol{X_2}$) derived from the magnetic variance matrix $M_{\mu v} = \langle B_\mu B_v \rangle - \langle B_\mu \rangle \langle B_v \rangle$ where the subscriptsμ, v= 1, 2, 3 denote cartesian components along the X, Y, Z system. The corresponding eigenvalues for each eigenvector are λ_1, λ_2, λ_3 ($\lambda_1 \geq \lambda_2 \geq \lambda_3 \geq 0$).

Besides, the angular uncertainty of $\boldsymbol{X_1}, \boldsymbol{X_2}, \boldsymbol{X_3}$ can also be estimated as

$$|\Delta\varphi_{ij}| = |\Delta\varphi_{ji}| = \sqrt{\frac{\lambda_3(\lambda_i + \lambda_j - \lambda_3)}{(N-1)(\lambda_i - \lambda_j)^2}} \quad (2)$$

Here $|\Delta\varphi_{ij}|$ denotes the expected angular uncertainty of eigenvector $\boldsymbol{X_i}$ for rotation toward or away from eigenvector $\boldsymbol{X_j}$, while N is the number of data points.

The eigenvectors $\boldsymbol{X_1}$, $\boldsymbol{X_2}$, $\boldsymbol{X_3}$ are usually written as $\hat{\boldsymbol{L}}$, $\hat{\boldsymbol{M}}$, $\hat{\boldsymbol{N}}$ to represent the direction of maximum, intermediate and minimum variance of the magnetic field, respectively. The $\hat{\boldsymbol{N}}$ here is regarded as the normal to the CS. The accuracy of MVA results is inferred by the ratio of the corresponding eigenvalue $\lambda_1, \lambda_2, \lambda_3$. A high intermediate-to-minimum eigenvalue ratio (λ_2/λ_3) indicates that the normal vector is well determined for a given current sheet crossing. The larger the ratio is, the more accurate the yielded normal becomes.

For further analysis, the normal $\hat{\boldsymbol{n}}$ is chosen as the vector which always points form $+B_X$ to $-B_X$ hemisphere. Thus, the normal is given by

$$\hat{\mathbf{n}} = \mathrm{sgn}(-\Delta B_X)\ \mathrm{sgn}\left(\hat{\mathbf{v}}_t \cdot \hat{\mathbf{N}}\right) \hat{\mathbf{N}} \tag{3}$$

Where sgn is the sign function, $\hat{\mathbf{v}}_t$ represents the velocity vector of MAVEN, and $\Delta B_X > 0$, if B_X change from $-B_X$ to $+B_X$, and vice versa.

3.2 Current Sheet Structure Shift Evaluation

To study the correlations between the flow-aligned component of IMF and the CS structure shift, the shift of the CS must be estimated with the IMF flow-aligned component taken into account.

Here an example method is presented to quantitively analyze the shift of CS structure. The CS is ideally assumed to be plane structure, and the solar wind flow is along the -X direction. As presented in Figure 1 in the YZ plane, the CS, if no shift occurs (see the thick blue line), would contain the Sun-Mars line, which projected onto the YZ plane is the point O, i.e., the equatorial center of the CS. In this case the size of the $+B_X$ hemisphere equals to that of the $+B_X$ hemisphere. Point P is an example of where a spacecraft could cross the CS. If the CS shifts toward either lobe (see the thin dashed blue lines), the lobe system becomes asymmetric and the crossing of the CS would occur at any of the points denoted as P′.

The angle, α, between the CS normal $\hat{n}$ and the position vector $\overrightarrow{OP}$ or $\overrightarrow{OP'}$ is ≈ 90° if no significant shift occurs, and α > 90° (α < 90°) if the CS is displaced toward the $+B_X$ hemisphere (-

B_X hemisphere). The shifted distance can be estimated as $\Delta d = |\overrightarrow{OP'}|cos\alpha$. The analysis on the shifted distance still holds on even $\hat{\boldsymbol{n}}$ has a significant n_X component. In this case, one just needs to replace $\hat{\boldsymbol{n}}$ by the cross-flow component $\hat{\boldsymbol{n}}_\perp$ to calculate the angle α, where $\hat{\boldsymbol{n}}_\perp$= (0**i**, n_y**j**, n_z**k**). It should be noted that no IMF condition is applied using this technique: thus, the shifted distance can be calculated without knowing the simultaneous upstream IMF condition. Further, considering the angular uncertainty of CS normal via equation (2), the uncertainty of the shifted distance can be estimated as well.

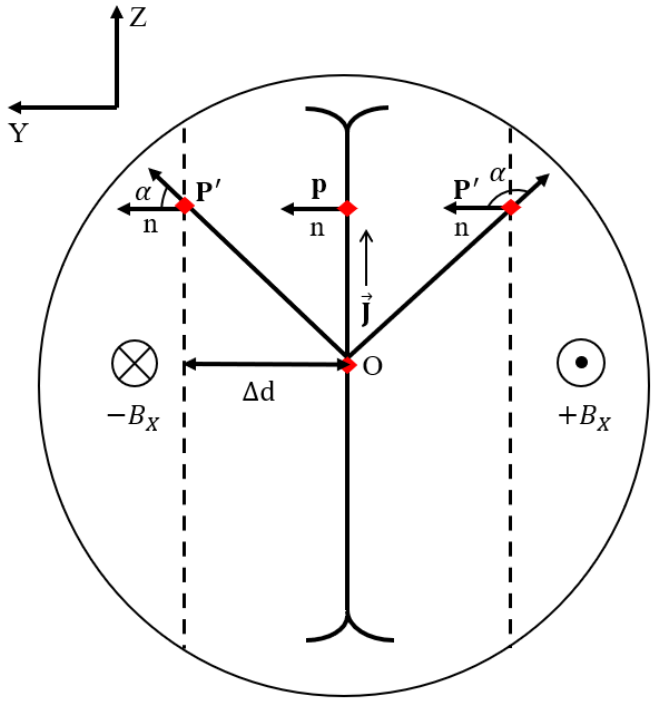

Figure 1. *The diagram illustrates the technique that evaluates the displacement of the CS. The thick blue line indicates the unshifted CS, and the CS crossing observed by MAVEN is at point P in this case. Similarly, the thin dashed blue lines represent a shifted CS, and the possible CS crossing points are the points P′. The CS normal at P or P′ is represented by* $\hat{\boldsymbol{n}}$ *which points from* $+B_X$ *hemisphere to* $-B_X$ *hemisphere always. The angle, α, between* $\overrightarrow{OP'}$ *and* $\hat{\boldsymbol{n}}$ *is larger (less) than 90° when CS is much displaced toward the* $+B_X$ *hemisphere (*$-B_X$ *hemisphere).*

4 Current Sheet Crossing Case Studies

To systematically analyze the possible influence of the IMF flow-aligned component on the CS structure, we firstly will study three cases with a significant sunward flow component, a dominant cross-flow component and a dominant tailward flow component respectively for comparison.

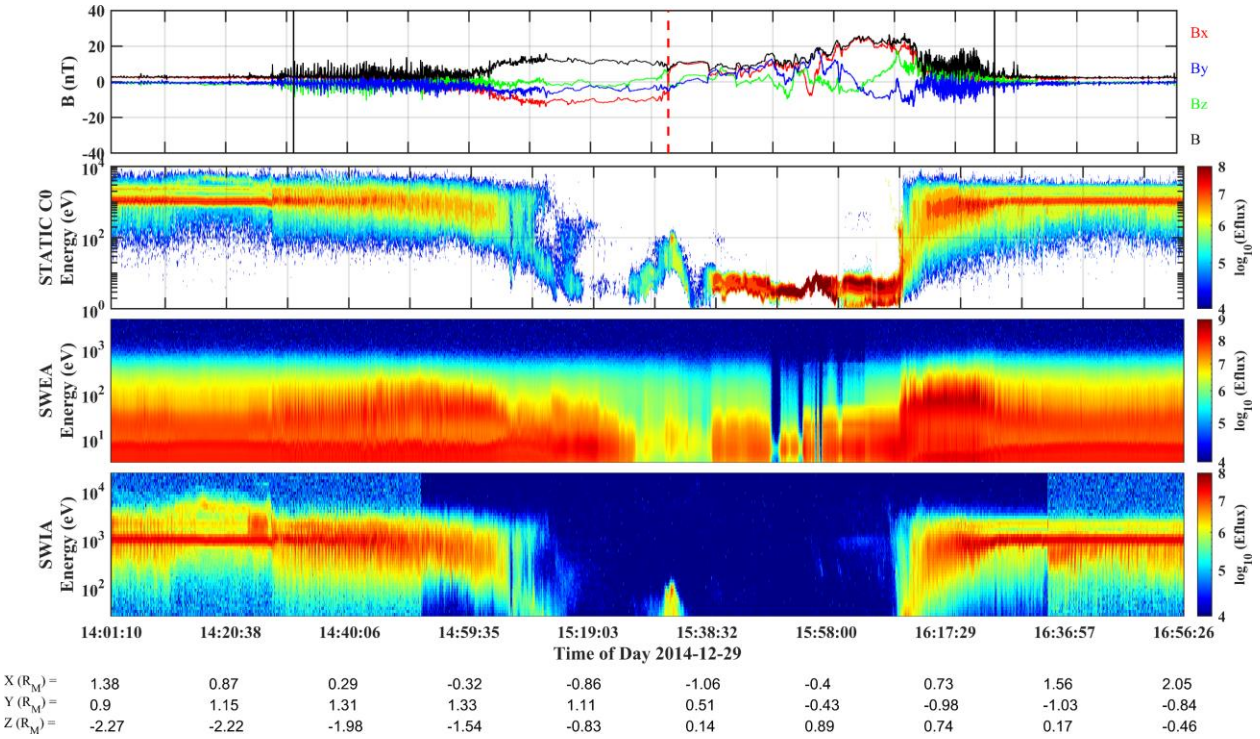

Figure 2. *MAVEN crossing of the Martian magnetosphere on 29 December 2014. (the first to the fourth panel) The time series of magnetic field, the energy-time spectrogram of ions, electrons, and of solar wind ions. The position of MAVEN in MSO is given below the panels. The crossings of the bow shock and the tail CS are labeled by vertical black and red lines, respectively.*

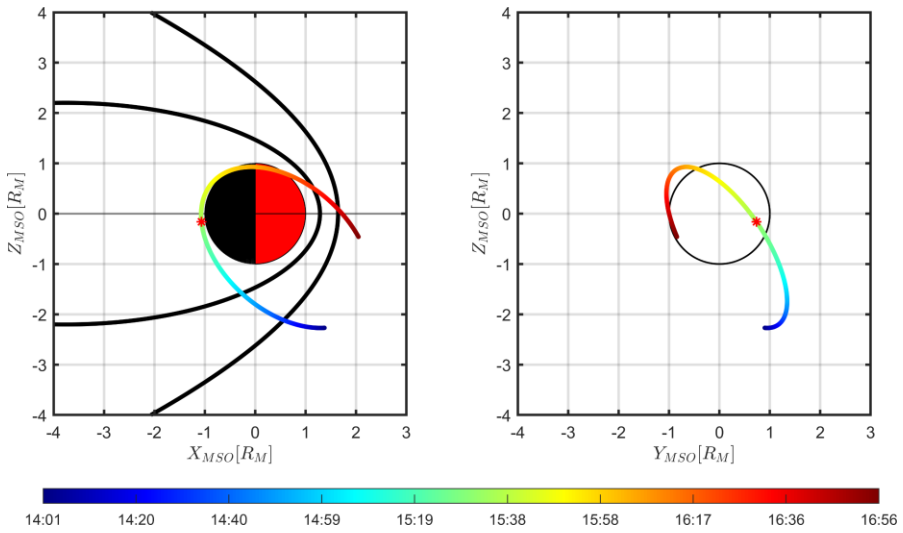

Figure 3. *MAVEN trajectory in the XZ plane (left) and YZ (right) plane on 29 December 2014. In the XZ plane, the nominal bow shock (BS) and induced magnetosphere boundary (IMB) are marked by the black lines [Vignes et al., 2000]. The red star marks the CS crossing and the color bar indicates the time.*

4.1 Case on 29 December 2014

As shown on Figure 2, MAVEN is crossing the Martian magnetosphere during 14:01-16:57 on 29 December 2014. The time series plot of data from MAG, STATIC, SWEA and SWIA is shown in Figure, which displays the magnetic field and its three components in MSO coordinates and the energy-time spectrogram of electrons and ions.

As seen in Figure 2, the MAVEN crossings of the bow shock are indicated by the vertical black lines with a jump of the magnetic field and the distinct changes in the plasma spectrograms [*Nagy et al*., 2004]. The average IMF 30 min before the inbound bow shock crossing is seen as $\boldsymbol{B_1}$= [2.52, -0.90, -0.48] nT, while the average IMF after the outbound bow shock crossing yields $\boldsymbol{B_2}$= [2.34, -0.22, -0.84] nT, so the average IMF during the MAVEN magnetospheric crossing is $(\boldsymbol{B_1} + \boldsymbol{B_2})/2$= [2.43, -0.56, -0.66] nT, the cone angle (the angle between the +X direction and the IMF direction) of the IMF is 19°. Evidently, the IMF's orientation is significantly sunward, the IMF is dominated by the $+B_X$ component. Besides, the IMF remained comparatively steady before and after the bow shock crossings (seen the steady IMF definition in Section 4.4).

The current sheet crossing is marked by the red dashed vertical line at 15:32:44 UTC, when MAVEN is located at [-1.07, 0.74, -0.16] R_M. The current sheet crossing is identified by the change

of the sign of B_X component, which changes from tailward to sunward. The current sheet crossing is also accompanied by the enhancement of the electron flux and ion flux [*Halekas et al*., 2006], which also indicate that MAVEN is indeed crossing the CS in the magnetotail.

Figure 3 illustrate MAVEN's trajectory from 14:01 UTC-16:56 UTC. Figure 3a provides a meridional plane view, while Figure 3b is the view from the tail toward the planet. The red stars present CS crossing. As described in Section 3, we performed the MVA method to the magnetic field data for the CS crossing and determined the CS normal direction. The MVA is applied to the magnetic field data at the CS crossing during 15:31:52-15:33:36, the maximum, intermediate and the minimum variance directions of the magnetic field are yielded as $\hat{\boldsymbol{L}}$= [0.86, -0.51 0.009], $\hat{\boldsymbol{M}}$= [-0.17, -0.30, -0.94], $\hat{\boldsymbol{n}}$ = [0.48, 0.80, -0.35], respectively. In addition, the corresponding eigenvalues are $\lambda_1 = 51.2$, $\lambda_2 = 1.22$, $\lambda_3 = 0.31$ based on the calculations.

Applied the analysis technique introduced in section 3.2, the shift of the CS structure is quantitively analyzed by calculating the angle, α, between the $n_\perp$ and the position of the observed CS crossing position vector. The $\alpha \approx 11^\circ$ based on the calculation and the shift distance of the CS can be estimated as $\Delta d \sim 0.73 R_M$, this indicates that the structure of CS is largely shifted towards the $-B_X$ hemisphere. In addition, as described in section 3.1 the accuracy of MVA results is inferred from the eigenvalues, the intermediate-to-minimum eigenvalue ratio here λ_2/λ_3=3.9, which indicates CS normal direction is well-determined. Apart from that, the distance of the crossing location to the equatorial plane is estimated as $R \sim 0.75 R_M$. Thus, based on the angular uncertainty of $\hat{\boldsymbol{n}}$ relative to the orientation of $\hat{\boldsymbol{M}}$ via equation (3), the range of the shift distance of CS can be $\Delta d \in [0.72, 0.74]\ R_M$. The related parameters regarding the corresponding crossings are tabulated in Table 1.

Table 1: The Parameters Related to the Current Sheet Crossing Cases.

Time	**Location[a] (R_M)**	**IMF[b]**	**Cone Angle[b]**	$\hat{\boldsymbol{n}}$	λ_2/λ_3	Δd^c
2014/12/29 15:32:44	**(-1.07, 0.74, -0.16)**	**(2.43, -0.56, -0.66)**	**20°**	**(0.48 0.79 -0.35)**	**3.92**	**0.73∈ [0.72, 0.74]**
2015/09/03 21:52:51	**(-1.19, -0.42, -0.38)**	**(-3.10, 6.52, 0.19)**	**115°**	**(-0.11 0.73 -0.68)**	**10.81**	**-0.05∈ [-0.08, -0.02]**
2018/02/19 00:47:08	**(-0.68, -1.12, -0.20)**	**(-1.94, -0.63, 1.24)**	**145°**	**(0.12 0.18 0.98)**	**3.95**	**-0.40∈ [-0.50, -0.29]**

a: The location of current sheet crossing in MSO coordinates.

b: The averaged IMF and its cone angle.

c: The shifted distance of the current sheet plane. The sign "-" (+) represents the current sheet is shifted toward the $+B_X$ ($-B_X$) hemisphere, and vice versa. The range of the shifted distance is show in the square bracket.

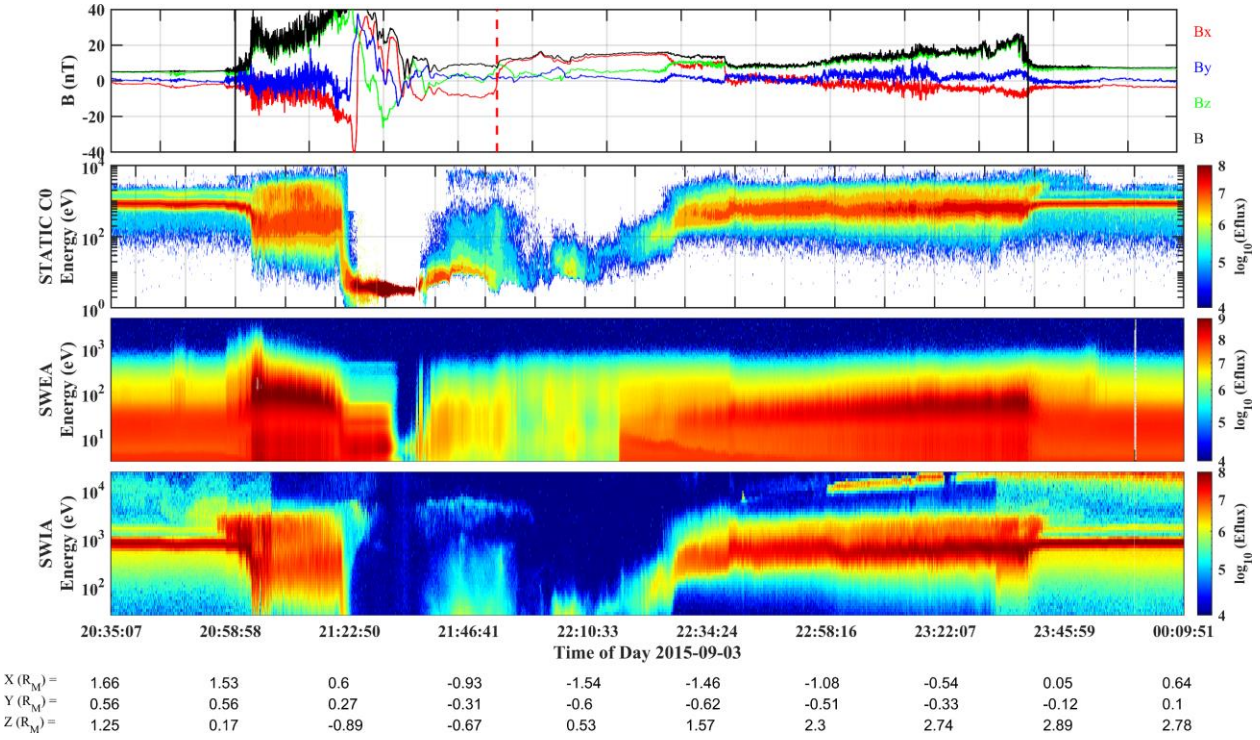

Figure 4. *MAVEN crossing of the Martian magnetosphere on 3 September 2015. (the first to the fourth panel) The time series of magnetic field, the energy-time spectrogram of ions, electrons, and of solar wind ions. The crossings of the bow shock and the tail CS are labeled by vertical black and red lines, respectively.*

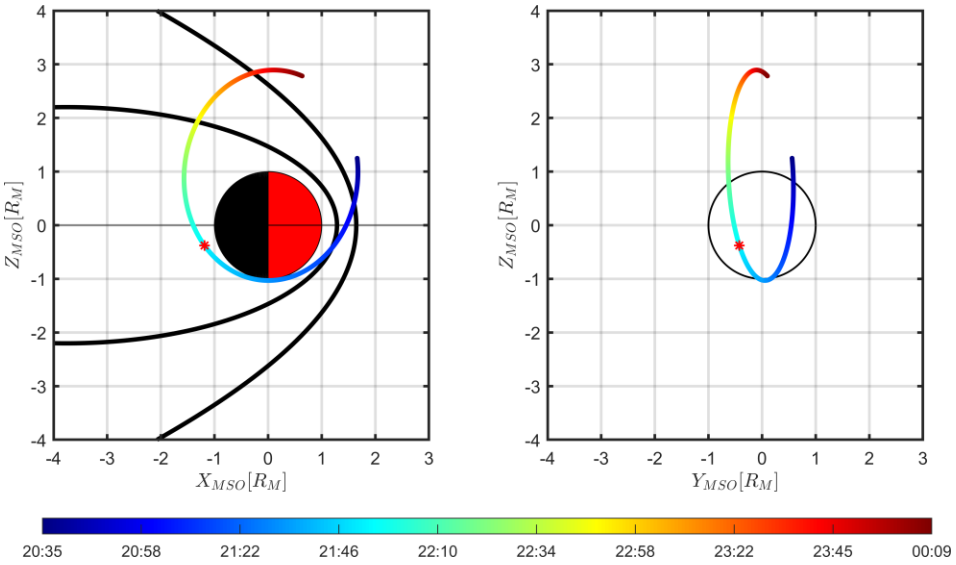

Figure 5. *The MAVEN's trajectory on 3 September 2015. The format is the same with Figure 3.*

4.2 Case on 3 September 2015

Another case is shown is Figure with a dominant cross-flow component, which occurred on 3 September 2015. Similarly, the vertical black lines mark the inbound and outbound bow shock crossings at 21:05:07 and 23:39:51 respectively along with the fluctuations of the magnetic field and the ion energy spectrogram. The 30 min average before the inbound bow shock crossing yields, $\boldsymbol{B_1}$= [-2.84, 6.22 0.27] nT, and $\boldsymbol{B_2}$= [-3.36, 6.83 0.11] nT for the 30 min average after the outbound crossing, so the average IMF is $(\boldsymbol{B_1} + \boldsymbol{B_2})/2$=[-3.10, 6.52, 0.19] nT. The cone angle of the average IMF is $\sim 115^{\circ}$, which indicates that the IMF is dominated by cross-flow component during the entire Martian magnetosphere crossing while the B_X remined very steady.

At 21:52:51 UTC, marked by the dashed red line, MAVEN is crossing the CS when located at [-1.19, -0.42, -038]R_M. The B_X component reverses from tailward to sunward as expected, along with the enhancement of ion flux and electron flux recorded by SWIA and SWEA instruments. Figure displays the trajectory of MAVEN in the XZ and YZ plane, the CS crossing is marked by red stars. As before, the MVA analysis is applied to the time interval 21:52:31- 21:53:11, the eigenvectors derived from the analysis are $\hat{\boldsymbol{L}}$= [0.98, 0.22, 0.08], $\hat{\boldsymbol{M}}$= [-0.21, 0.65, 0.73], $\hat{\boldsymbol{n}}$= [-0.11, 0.73, -0.68]. The corresponding eigenvalues are $\lambda_1 = 11.4$, $\lambda_2 = 0.0893$, $\lambda_3 = 0.00826$, respectively.

With the same analysis technique before, it is estimated that the location of the CS crossing to the equatorial center of the CS plane is $R{\sim}0.57\ R_M$. The deviation angle α, between the CS normal vector and the position vector is about 95°, so we find that shifted distance of the CS is $\Delta d{\sim}-0.05\ R_M$, which suggests that the CS does not shift significantly towards the $+B_X$ hemisphere under the cross-flow dominant IMF condition. Still, the uncertainty of the shifted distance can be estimated by equation (3), the range of the CS shifted distance can be derived as $\Delta d \in$ [-0.08, -0.02] R_M.

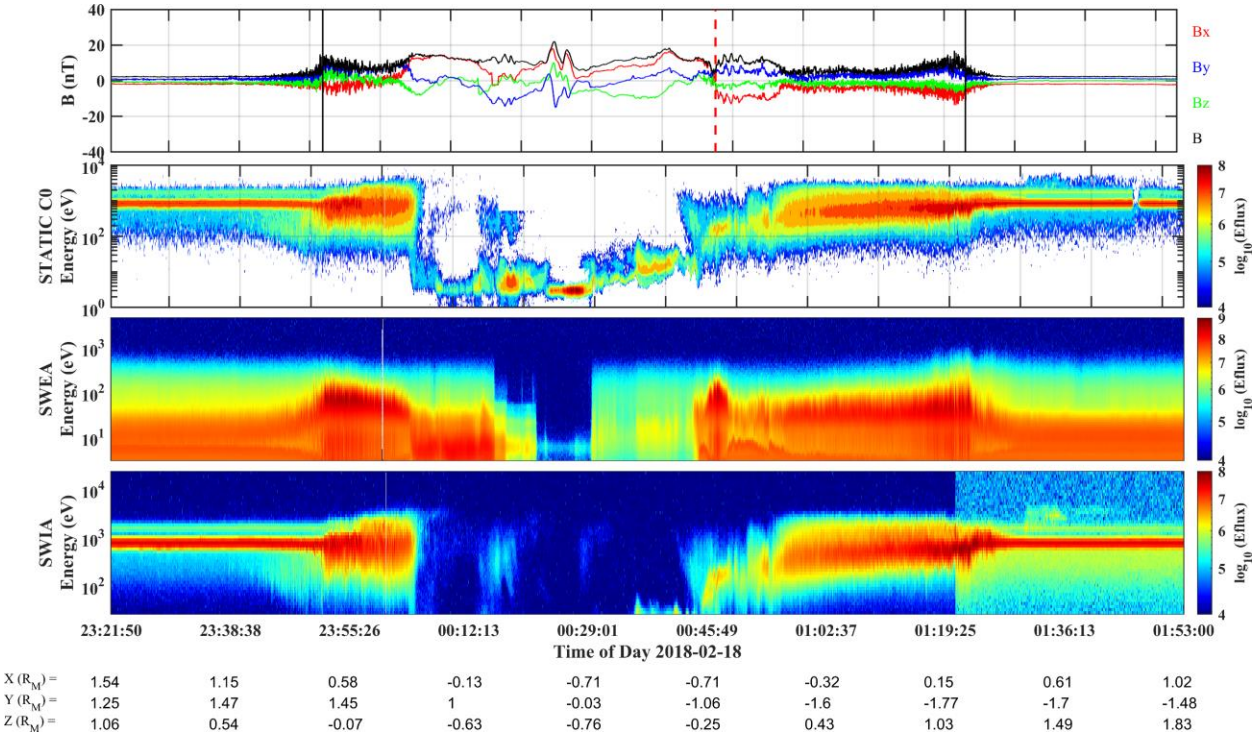

Figure 6. *MAVEN crossing of the Martian magnetosphere on 18 and 19 February 2018. (the first to the fourth panel) The time series of magnetic field, the energy-time spectrogram of ions, electrons, and of solar wind ions. The crossings of the bow shock and the tail CS are labeled by vertical black and red lines, respectively.*

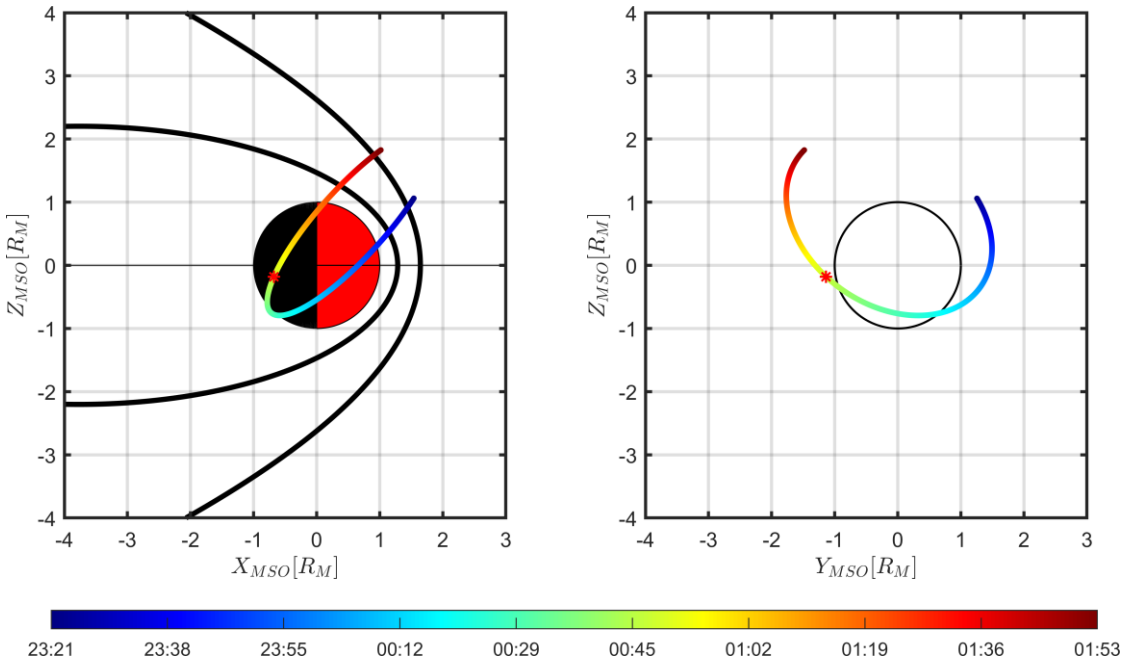

Figure 7. *The MAVEN's trajectory on 18 and 19 February 2018. The format is the same with Figure 3.*

4.3 Case on 19 February 2018

As expected, Figure 6 shows a case with dominant tailward IMF B_X. In Figure 6, the vertical black lines represent the bow shock crossings at 23:51:50 and 01:23:00, respectively. The 30 min averaged IMF before the inbound bow shock crossing is $\boldsymbol{B_1}$= [-1.81, -0.92, 1.22] nT, while the averaged IMF after outbound crossing is $\boldsymbol{B_2}$= [-2.13, -0.33, 1.25] nT, the corresponding IMF is [-1.97, -0.63, 1.24] nT and the cone angle is 145°. Clearly, the IMF is significantly tailward during the crossing of the Martian magnetosphere.

The CS crossing is marked by vertical red line at 00:47:08 when MAVEN is located at [-0.68, -1.12 -0.2]R_M, the sign of magnetic field B_X component changes along with the enhancement of energetic electron and ion flux. The MVA is applied over the interval 00:46:44- 00:47:32 during the magnetotail CS crossing event, the yielded eigenvectors are $\hat{\boldsymbol{L}}$= [0.98, -0.19, -0.08], $\hat{\boldsymbol{M}}$= [-0.17, -0.97, 0.20], $\hat{\boldsymbol{n}}$= [0.12, 0.18, 0.98]. The corresponding eigenvalues are $\lambda_1 = 11.8$, $\lambda_2 = 3.3$, $\lambda_3 = 0.84$, respectively. Then we calculated the deviation angle α between the $\widehat{n_{\perp}}$ and the position vector, which is 111°. The shifted distance can be estimated based on the angle as $\Delta d \sim -0.40\ R_M$, which suggests the CS plane is largely displaced toward $+B_X$ hemisphere under the tailward

dominant IMF condition. Considering the angular uncertainty of $\hat{\boldsymbol{n}}$ relative to the orientation of $\widehat{\boldsymbol{M}}$, the range of the CS shifted distance is estimated as $\Delta d \in$ [-0.50, -0.29]R_M.

In summary, the analysis based on the selected three cases suggests that the IMF B_X seems to result in a systematic shift of the current sheet and a corresponding asymmetry of the structure. However, the selected cases cannot help us determine the possible correlations between the CS displacement and the IMF orientation. In that case, we enlarge the study with more cases based on the selection criteria described in the following subsection

Table 2: The table format is the same as Table 1 with more current sheet crossing cases.

Time	Location[a] (R_M)	IMF[b]	Cone Angle[b]	$\hat{n}$	λ_2/λ_3	Δd^c
2014/12/29 15:32:44	(-1.07, 0.74, -0.16)	(2.43, -0.56, -0.66)	20°	(0.48 0.79 -0.35)	3.93	0.73∈ [0.72, 0.74]
2015/09/03 21:52:51	(-1.19, -0.42, -0.38)	(-3.10, 6.52, 0.19)	115°	(-0.11 0.73 -0.68)	10.81	-0.05∈ [-0.08, -0.02]
2018/02/19 00:47:08	(-0.68, -1.12, -0.20)	(-1.94, -0.63, 1.24)	145°	(0.12 0.18 0.98)	3.95	-0.40∈ [-0.50, -0.29]
2014/12/22 09:28:21	(-1.21, 0.55, -0.15)	(2.77, -3.24, -3.20)	59°	(-0.03 0.97 -0.24)	11.91	0.57∈ [0.56, 0.57]
2015/08/31 20:01:48	(-1.17, -0.49, -0.34)	(0.47, 4.43, -0.98)	84°	(0.22 -0.47 -0.85)	10.28	0.53∈ [0.52, 0.55]
2015/09/29 09:09:28	(-1.55, 0.14, -0.41)	(0.23, 2.19, -0.06)	84°	(-0.01 0.40 -0.92)	11.59	0.43∈ [0.430, 0.432]
2018/04/03 11:23:17	(-1.33, 0.15, -0.4)	(-0.19, -2.13, -0.06)	95°	(-0.23 -0.37 -0.90)	8.17	-0.43∈ [-0.43, -0.43]
2014/12/04 06:00:12	(-1.47, 0.05, -0.25)	(-0.58, 3.47, -1.56)	99°	(0.18 0.45 -0.88)	1.64	0.25∈ [0.23, 0.25]
2017/07/09 19:53:59	(-1.32, 1.08, -1.52)	(-3.10, 6.52, 0.19)	103°	(-0.29 -0.93 0.23)	4.47	-0.68∈ [-0.85, -0.43]
2014/12/05 09:40:14	(-1.30, -0.10, 0.13)	(-3.84, 2.98, -0.87)	141°	(0.23 0.97 -0.09)	5.33	-0.11∈ [-0.12, -0.10]
2016/02/02 11:02:04	(-1.00, -0.82, -0.31)	(-4.73, 0.61, 1.73)	159°	(0.33 0.85 0.42)	5.40	-0.87∈ [-0.88, -0.87]
2016/03/05 03:56:42	(-1.20, -0.12, 0.48)	(-1.34, -0.29, -0.59)	154°	(-0.73 0.1 -0.68)	9.31	-0.49∈ [-0.50, -0.49]
2018/03/14 12:41:51	(-1.17, -0.40, -0.39)	(-2.04, 1.41, 0.53)	144°	(0.17 0.91 -0.37)	10.71	-0.22∈ [-0.25, -0.20]
2016/08/15 20:30:25	(-1.10, -0.12, 0.37)	(3.28, 0.70, 1.31)	24°	(-0.35 -0.67 0.65)	15.52	0.34∈ [0.34,0.35]

a: The location of current sheet crossing in MSO coordinates.

b: The averaged IMF and its cone angle.

c: The shifted distance of the current sheet plane. The sign "-" (+) represents the current sheet is shifted toward the $+B_X$ ($-B_X$) hemisphere, and vice versa. The range of the shifted distance is show in the square bracket.

4.4 More cases

To systematically analyze whether the flow-aligned component can impact the CS structure and cause the asymmetry in Martian magnetotail, more CS crossing cases are selected for the analysis. The magnetic field data of MAVEN with a 1-s time resolution from October 2014 to February 2020 are adopted to select good current sheet crossing cases. The selection criteria are as followed:

1. MAVEN should be located in Martian magnetotail region, with region confinement $-3R_M < X < -0.5R_M$, $\rho = \sqrt{Y^2 + Z^2} < 1.3R_M$.
2. The CS crossings during the MAVEN magnetospheric crossings can be identified by the change of B_X sign along with the enhancement of ions and electrons flux [*Halekas et al*., 2006]. The CS should be assumed as stationary enough during the crossing, so evident flapping event of the CS should not occur during the crossing [*Rong et al.*, 2015a, 2015b; *DiBraccio et al.*, 2017] and the CS crossing should only occur one time during the magnetotail crossing. In that case, further analysis of the CS structure shift can be made.
3. To get steady IMF crossings, the upstream IMF component should fulfill the steady criteria [*Rong et al.*, 2014, 2016]: the 30 min averaged IMF before the inbound bow shock crossing are denoted as $\boldsymbol{B_1}$, while $\boldsymbol{B_2}$ represents the 30 min averaged IMF after the outbound bow shock crossing (A list of MAVEN bow shock crossings from October 2014 to February 2020 can be found in the supporting information). The criteria regarding angle and strength should be fulfilled to meet the steady requirement: the deviation angle α between $\boldsymbol{B_1}$ and $\boldsymbol{B_2}$ should be less than 30° and the perturbations of IMF strength should satisfy $\frac{2\|\mathbf{B_1}|-|\mathbf{B_2}\|}{|\mathbf{B_1}|+|\mathbf{B_2}|} < 0.2$. Then the averaged upstream IMF of the MAVEN crossing is $(\boldsymbol{B_1} + \boldsymbol{B_2})/2$.
4. To make the better analysis, no large fluctuations should occur in the upstream IMF: we visually picked out the good CS crossing cases from all the magnetospheric crossings which the IMF 30 min before the bow shock inbound crossing and after the outbound crossing show no evident fluctuations.

5. To avoid the potential influence of the crustal magnetic fields, the CS crossing should be above at least 400 km when MAVEN flying above the strong crustal magnetic field regions.

More cases (total 14 cases) were selected for studies based on the above criteria, the related parameters regarding the CS crossing are tabulated in Table 2. Based on the analysis of these cases, Figure 8 shows the shifted distance Δd of CS as a function of the upstream IMF cone angle. A correlation can be seen between the shifted distance and the IMF cone angle, the shifted distance varies inversely with the IMF cone angle, that is the shifted distance $|\Delta d| \gg 0$ when the IMF cone angle is much less or more than 90°, and vice versa. However, the inverse correlation is not evident for two of the selected cases. The ratioλ_2/λ_3 of case one with cone angle 99° is 1.6, so the reason accounted for this inconsistency may be the less well-determined current sheet normal direction estimated by the MVA. While the inconsistency of another case may be caused by other unknown reasons, since some other factors may also displace the current sheet structure to some degree. From the results of the carefully selected CS crossing cases, there seems to be a correlation between the displacement of the CS structure and the IMF cone angle. The CS would be shifted more to the +Y direction, when the IMF cone angle is much less than 90°, while the CS would be largely shifted to the -Y direction, when the IMF cone angle is much greater than 90°.

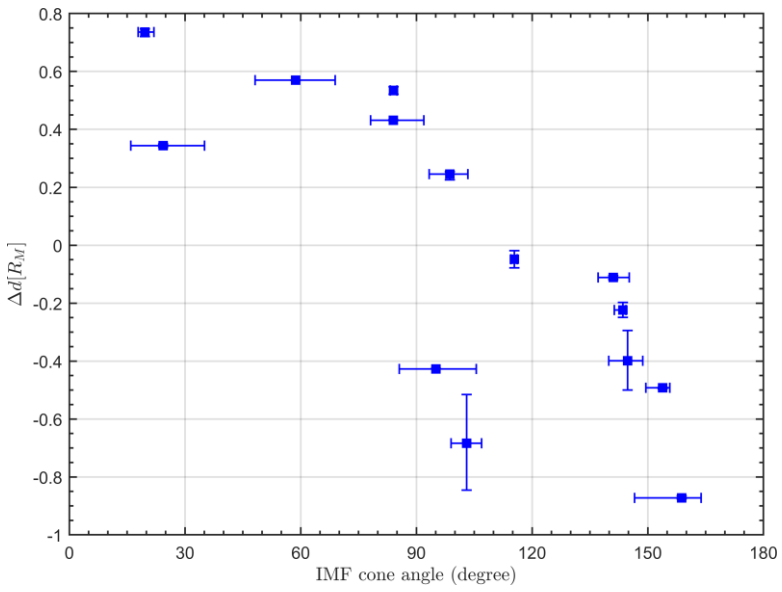

Figure 8. *Scatter plot represents the shifted distance of the CS as a function of the IMF cone angle. The lengths of the horizontal error bars represent the IMF cone angle deviation between the IMF*

for inbound and outbound bow shock crossings. The lengths of the vertical error bars represent the uncertainty of the shifted distance from the uncertainty of the CS normal estimated by the MVA.

5 Statistical Analysis

Analysis based on selected CS crossing cases suggest the possible inverse correlation between the shifted distance of the CS and the cone angle of upstream IMF. However, one may argue that the biased selection of the CS crossing cases would make the results unreliable. As a result, it is of great importance to statistically check the effects of the IMF flow-aligned component (B_X) on the average configurations of the CS structures in magnetotail. To statistically study the influences of the IMF, the magnetic field data of MAVEN MAG from October 2014 to February 2020 are adopted to the analysis.

The statistical analysis is made in Mars-Solar-Electric field (MSE) coordinate system. This involves a transformation in the Y-Z plane by calculating the direction of the solar wind convection electric field ($\boldsymbol{E_{SW}}$) on the basis of the anti-sunward solar wind flow ($\boldsymbol{V_{sw}}$) in the $-X_{MSO}$ direction and IMF orientation ($\boldsymbol{B_{IMF\_YZ}}$) perpendicular to the solar wind flow:$\boldsymbol{E_{SW}} = -\boldsymbol{V_{sw}} \times \boldsymbol{B_{IMF\_YZ}}$. $\boldsymbol{E_{SW}}$ is positive along the Z_{MSE} direction, and therefore $-\boldsymbol{V_{sw}}$ and $\boldsymbol{B_{IMF\_YZ}}$ oriented in the direction of X_{MSE} and Y_{MSE}, respectively. In MSE coordinates, the Z_{MSE} axis is basically contained in the CS plane which is nominally located at $Y_{MSE}\sim 0$.

Similar as the previous analysis, the procedures implemented in previous studies [*Rong et al*., 2014, 2016] are adopted which is, we select orbits when the upstream IMF satisfy the steady requirements defined in section 4.4 (there are total 1445 magnetospheric crossings fulfilling the criteria), and then the MAVEN magnetic field data are transformed into MSE coordinates with region confinement ($-3R_M < X_{MSE} < -0.5R_M$). Here the MSE coordinate system is computed using the averaged upstream IMF ($\boldsymbol{B} = (\boldsymbol{B_1} + \boldsymbol{B_2})/2$) and the corresponding solar wind velocity measured by SWIA.

To find the average configurations of the CS structure, we look at the B_X component spatial distributions in the MSE Y-Z plane and the size of the spatial bins are $0.2\times 0.2R_M$. We further compute the contours of B_X=0 in the plane. The contours of B_X=0 near $Y_{MSE}\sim 0$ can be seen as the average configuration of the CS structure. To analyze the IMF flow-aligned component effects on the CS configurations, the investigations are carried out under different IMF conditions, the

significant sunward IMF (cone angle <60°, 500 magnetospheric crossings) and tailward IMF (cone angle> 120°, 260 magnetospheric crossings), along with the cross-flow IMF (70° <cone angle<110°, 439 magnetospheric crossings). Figure 9 shows the spatial distributions of the IMF B_X in the MSE coordinates, Figure 9 (a)-(c) corresponds the sunward, tailward and cross-flow IMF condition respectively. In addition, the contours of B_X=0 are generated automatically by the MATLAB with an interpolation technique of its own, therefore the contour will pass through some spatial bins where $B_X \neq 0$ unavoidably. It should be noted that some "circle structure" of the contours appear in the lobe, there are no particular meanings for these circles, they are likely to be produced by the IMF uncertainty in some cases.

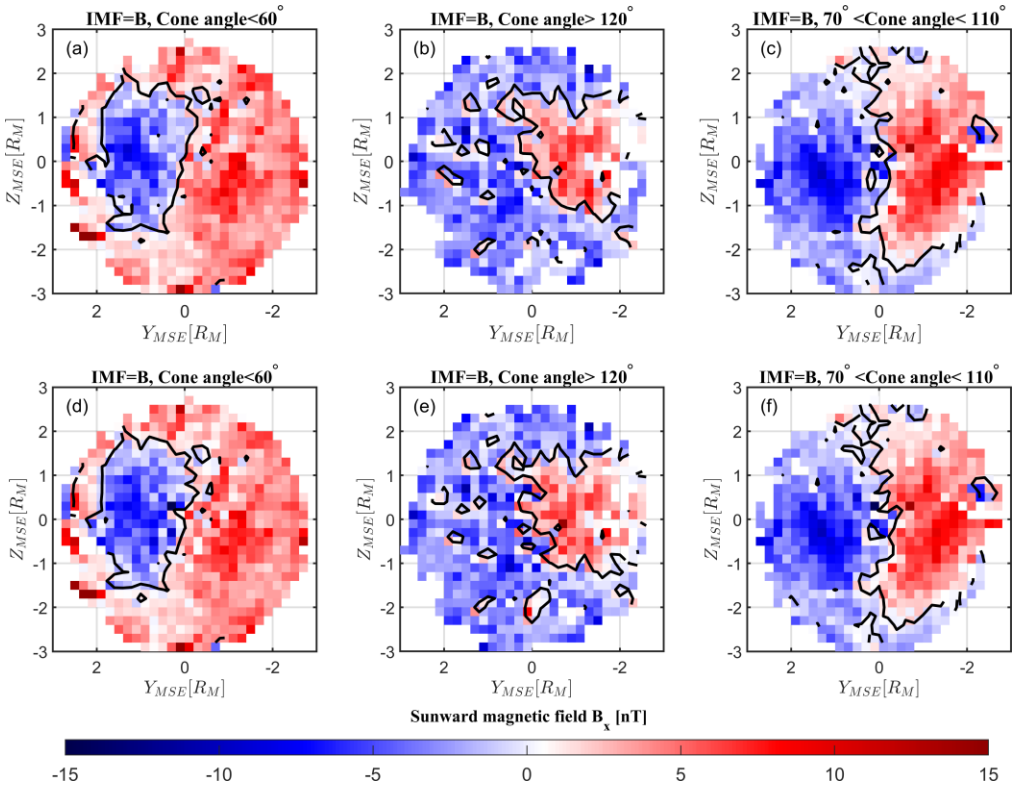

Figure 9. *The distribution of the B_X component in the modified Mars-Solar-Electric field (MSE) coordinates ($-3\ R_M < X_{MSE} < -0.5\ R_M$) when the average upstream IMF (**B**= (**B1**+**B2**)/2) is significantly (a) sunward (cone angle <60°) and (b) tailward (cone angle >120°) (c) cross-flow (70°< cone angle <110°). The average configurations of the tail current sheet structure are marked by the solid black lines. (a)-(c) represent the current sheet configurations without crustal*

magnetic fields effects. (d)-(f) represent the current sheet configurations with crustal magnetic fields effects.

To also look at the influence of the crustal fields, the average CS configurations under the crustal fields considered and omitted conditions are compared as well in this statistical study. To filter out the influence of the strongest crustal magnetic fields, we discarded magnetic field data recorded by MAVEN when it is flying above the strongest crustal fields region ($130^{\circ} - 230^{\circ}$ in longitude of the southern hemisphere) in the magnetotail region. Figure 9 (d)-(f) corresponds the sunward, tailward and cross-flow IMF condition with strong crustal magnetic fields considered. Considering the limited coverage of the crustal magnetic field effects, we also compared the crustal field effects at the near Mars magnetotail using the different region confinement ($-1.5R_M < X_{MSE} < -0.5R_M$) as shown in Figure 10.

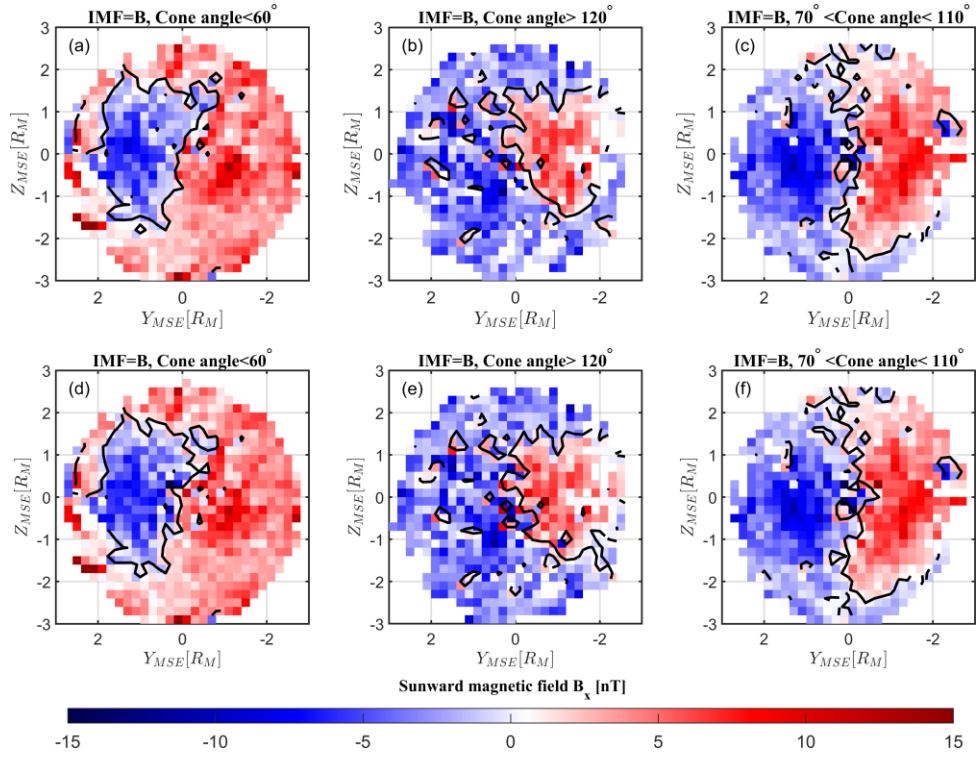

Figure 10. *The distribution of the B_X component in the modified Mars-Solar-Electric field (MSE) coordinates ($-1.5\,R_M < X_{MSE} < -0.5\,R_M$) when the average upstream IMF (**B**= (**B1**+**B2**)/2) is significantly (a) sunward (cone angle <60°) and (b) tailward (cone angle >120°) (c) cross-flow (70°< cone angle <110°). The average configurations of the tail current sheet structure are marked by the solid black lines. (a)-(c) represent the current sheet configurations*

without crustal magnetic fields effects. (d)-(f) represent the current sheet configurations with crustal magnetic fields effects.

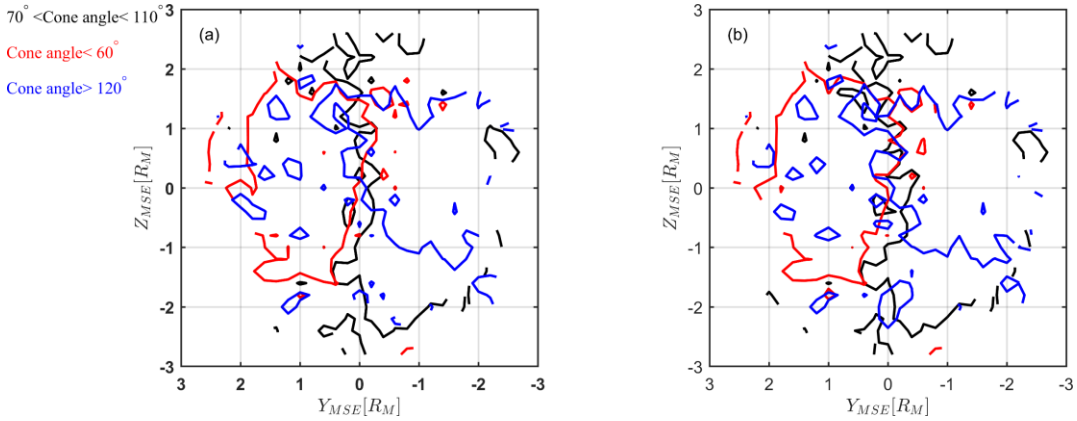

Figure 11. The average configuration of the magnetotail current sheet (the contour of B_X = 0 near Y_{MSE} ~ 0) when IMF is significantly sunward (red lines), tailward (blue lines) and cross-flow (black line).

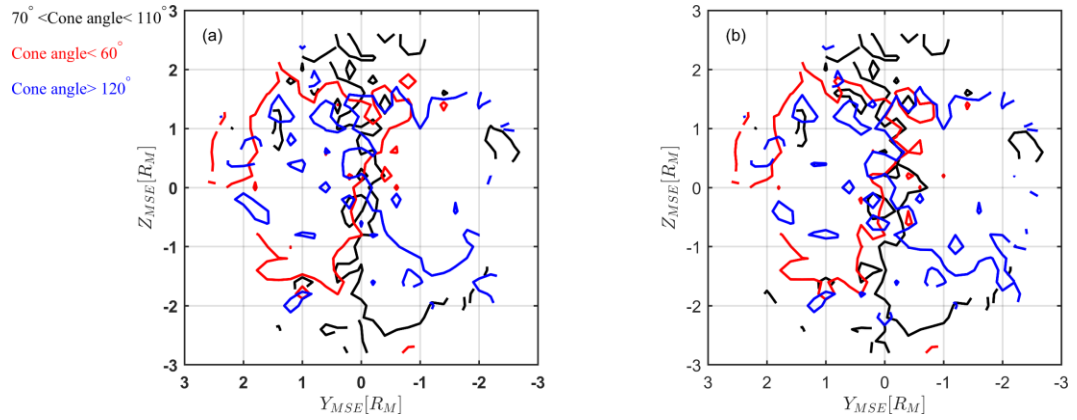

Figure 12. *The format is the same as Figure 11, with region confinement* ($-1.5\ R_M < X_{MSE} < -0.5\ R_M$).

As shown in Figure 9 and Figure 10, the contours represent the average configurations of the CS. The structure of the CS, however, is not always aligned with the solar wind motional electric field ($\boldsymbol{E_{SW}}$) as one would expect, the average configurations of the CS are actually sensitive to the value of the IMF cone angle, which suggests that the structures of the CS are influenced by the

flow-aligned component of the IMF. Moreover, the offset of the CS structure is systematically controlled by the IMF, the CS is shifted to the dusk (+Y) when the IMF is significantly sunward $+B_X$ hemisphere, and shifted to the dawn (-Y) when the tailward IMF is dominant and resulting in a dominant $-B_X$ hemisphere of the magnetic lobes, while the CS is nearly located at $Y_{MSE}\sim 0$ during the cross-flow dominant IMF conditions, and the situations are nearly identical for the observations made in the near Mars magnetotail region ($-1.5\,R_M < X_{MSE} < -0.5\,R_M$). Considering the effects from the crustal fields, the general configurations of the CS are similar when the crustal fields are included, there are indeed some minor changes in the CS structures near $Z_{MSE}\sim 0$ where the strong crustal magnetic fields are present. As for the near Mars magnetotail, the average configurations of the CS tend to be much more variant, part of the curves are offset when the crustal fields are included, the comparison between the included and excluded crustal fields observations further confirm the effects of crustal fields on current sheet configurations in Martian magnetotail. [*Halekas et al*., 2006; *Luhmann et al.,* 2015]. But from our statistical studies, we can tell that the shift of the current sheet structure is dominated by the flow-aligned component of IMF systematically, but still with some minor contributions from the crustal magnetic fields.

Moreover, *Liemohn et al*. [2017] found the asymmetry of the current sheet may also be controlled by ionospheric conditions, the current sheet is shifted to the dawn (-Y) during solar maximum and to the dusk (+Y) during solar minimum. Their MHD simulation results suggest the shift is not a function of crustal fields or solar wind conditions, since they are omitted and held constant in their study. Based on their study, we also roughly considered the effects of solar EUV intensity, due to the limited operation time length of MAVEN, we choose the perihelion (1.38-1.52 AU) and aphelion (1.52-1.66 AU) to compare the solar EUV intensity effects. The configurations of the CS are slightly different in when considering the solar EUV intensity effects, but as still the IMF flow-aligned component is the dominant factor for current sheet configuration shift (Figures presented in supplementary files). We cannot conclude whether the configuration differences are caused by solar EUV intensity or the change of IMF conditions, so further quantitative studies on the solar EUV intensity effects on current sheet structure shift based on MAVEN observations may be required in the future to confirm that.

Based on above results, the statistical studies we carried out above support our conclusions from the selected individual cases: the shift of the current sheet structure in Martian magnetotail is

dominantly controlled by the flow-aligned component of IMF (B_X), with contributions from other factors like the crustal magnetic fields.

6 Discussion and Conclusions

In this work, based on carefully selected cases as well as statistical studies using MAVEN magnetic field data from October 2014 to February 2020. We found an appreciable dependence between the shift of the current sheet structure and the flow-aligned component of the IMF. The Mars magnetotail current sheet is located shifted toward the +Y side for the significant sunward IMF cases and then moves to the -Y side of the -X axis for the tailward IMF cases, while cross-flow dominant IMF cannot significantly displace the current sheet structure in Martian magnetotail. Besides, by comparing the average configurations of magnetotail current sheet structure derived from the crustal magnetic fields discarded data set and the normal data set, it is showed the current sheet structure can indeed be influenced by the crustal magnetic fields, as previous studies suggested [*Ma et al.*, 2002; *Harnett and Winglee*, 2005; *Fang et al.*, 2010, 2015; *Dong et al*., 2015]. Moreover, from the comparison we can tell that the dominant controlling factor for magnetotail current sheet structure is still the IMF orientation with some contributions from other factors, even though the effects from the crustal magnetic fields may be averaged to some degree.

Our study demonstrates that the dominant IMF B_X does show a correlation with the significant CS displacement and the corresponding lobe asymmetry of the magnetic field structure. However, some further discussions will be needed to present possible explanations accounted for inconsistence between previous results and our study, to point out the differences between the space environment of Venus and Mars. With the similar analysis technique, the study by *Rong et al*. [2016] found no evident correlations between the IMF orientation and asymmetries of the magnetic field structure in near-Venus magnetotail. Their results are inconsistent with the study by *McComas et al*. [1986], they gave two possible explanations for the inconsistence (see their discussion and conclusion): 1. The asymmetry may be caused other unknown reasons (e.g., the biased data set of PVO, since PVO spent little time measuring the upstream solar wind and IMF) 2. The IMF B_X can impact magnetic field structure, but not significant in near-Venus magnetotail where their observations were made. However, in our study the systematic asymmetry of current sheet structure controlled by the IMF can still be observed by MAVEN in the near-Mars magnetotail. Here we attempt to present some simple physical interpretations and discuss the

possible reasons accounted for the difference from the perspective of both the numerical simulations and theoretical analysis.

A previous study by *Romanelli et al*. [2014] presented the theoretical analysis between the interaction of the solar wind and the unmagnetized planets. They analytically addressed an ideal non-collisional interaction between conducting obstacles and magnetized plasma winds, where a perfectly magnetized magnetohydrodynamic (MHD) plasma (no resistivity) under steady state conditions flows around a spherical body for various orientations of the streaming magnetic field. The arbitrary orientation of the magnetic field was seen as the combination of a linear combination of the flow-aligned component and the cross-flow component in their study. Most of the structures and characters of the induced magnetosphere (e.g. the classical draping configuration) can be reproduced by their approach. Moreover, they found that when the external magnetic field is strictly perpendicular to the direction of the flow, the induced magnetotail formed downstream from the obstacle consists of two mirror-symmetric magnetic hemispheres separated by a flat PRL (polarity reverse layer, actually the magnetotail current sheet), the PRL is always in the same plane regardless of the orientation of the background magnetic field. In other words, the PRL cannot be displaced by the flow-aligned component of the magnetic field, which is consistent with the observations by *Rong et al.* [2016]. In addition, the IRPL (inverse polarity reverse layer, the boundary layer of magnetotail) appears when the there is a significant flow-aligned component in the magnetic field, and the IRPL also appears in IMF B_X dominant case 1 and case 2 in Venus magnetotail of *Rong et al*. [2016] (see Figure 5). It should be noted that *Romanelli et al*. [2014] only addressed the ideal MHD case without any resistivity. However, another work by *Romanelli et al*. [2015] (see their introduction) suggested that the inclusion of resistivity must result in a shift of the tail current sheet as *McComas et al*. [1986].

Apart from theoretical analysis, results from simulations (e.g. hybrid simulations and MHD simulations) can also help us interpret the possible reasons accounted for different magnetotail configurations. As mentioned in Introduction, the nonideal MHD simulation of Venus space environment (with particle collisions and resistivity) by *Ma et al*. [2013] showed the flow-aligned component of the IMF influences the magnetic field configuration of Venusian magnetotail systematically, which is consistent with our observations. In addition, the hybrid simulation of Titan by *Simon et al*. [2009] also showed that the dominant flow-aligned magnetic field component goes along with the corresponding asymmetry of Titan's magnetotail. Therefore, the nonideal

MHD simulations as well as the hybrid simulations show good agreement with our observations, suggesting the possibility that particle collisions and effects of resistivity favor a displacement of magnetotail current sheet under dominant IMF B_X conditions. Moreover, the simulation results mentioned above do not align with *Romanelli et al*. [2014] and *Rong et al*. [2016]. Based on that, we may infer the difference between the space environment of Mars and Venus, which is the resistivity effects may not be significant for near-Venus magnetotail formation compared with near-Mars magnetotail. In that case, we need to further discuss the results from ideal MHD simulations.

The results from ideal MHD simulations [*Zhang et al.*, 2009] showed that the induced magnetosphere of Venus totally disappear under the extreme flow-aligned IMF orientation. The field lines are excluded from the Venus wake. The simulation results are understandable, since the flow-aligned magnetic field upstream must indicate a flow-aligned downstream according to MHD Rankie-Hugoniot conditions. If the IMF can simply be seen as the linear combination of the flow-aligned and cross-flow component as is the case in the ideal problem addressed by *Romanelli et al*. [2014], the results of *Rong et al*. [2016] are easy to be interpreted. Any IMF orientation can be decomposed into a cross-flow component and a flow-aligned component (IMF B_X). In terms of ideal MHD, the flow-aligned component cannot penetrate into magnetotail, only cross-flow can contribute to the formation of magnetotail. Thus, the results of *Rong et al.* [2016] suggested that the flow-aligned dominant IMF cannot significantly influence the magnetotail, since the solar wind can be seen as the steady state in their statistical studies based on their selection criteria, which perfectly satisfied the assumption of *Romanelli et al*. [2014], so their observations of near-Venus magnetotail can be interpreted by the ideal MHD situation.

Based on above discussion, we may infer the possible reason accounted for the inconsistence between our observations and previous study [*Rong et al.,* 2016, Figure 11]. From the perspective of theoretical analysis and numerical simulations, the different significance of particle effects and resistivity on Mars and Venus may play a role in the magnetotail shift. For Venus, neither the hybrid nor the MHD simulation is consistent with the observation by *Rong et al.* [2016], so it may imply that either the related particle effects, e.g., particle collisions and wave particle interaction, cannot significantly impact the magnetic field structure of Venusian magnetotail or some unknown effects other than the IMF Bx component that gives the shift and asymmetric structure of CS may balance the particle effects to make the CS unshifted significantly. For Mars, due to the smaller

ion gyroradius and effects from crustal magnetic fields, the related particle effects may play a more important role in the near-Mars magnetotail. In that case, particle collisions and effects of resistivity may indeed favor a displacement of magnetotail current sheet under dominant IMF B_X conditions. In all, the inconsistence between the observations of near-Mars and near-Venus magnetotail are possibly related to different particle effects of the planetary space environment, based on results from numerical simulations, theoretical analysis along with satellite observations.

In conclusion, the comparison of theoretical analysis and numerical simulations show that when the particle effects in the form of resistivity are included, the magnetotail current sheet would be systematically controlled by the IMF orientation as shown in our observations of near-Mars magnetotail. While in *Rong et al.* [2016], the statistical study suggested the effects of resistivity appearing in the models do not play a significant role in the formation of near-Venus magnetotail. The different results between Mars and Venus may imply the different role of particle effects in the magnetotail of the two planets, further simulation and observation will be needed to confirm the effects. Moreover, the displacement of current sheet following the orientation of the IMF has also consequences on the location of the region where planetary particle acceleration is expected. Therefore, the displacement of the current sheet structure should be taken into account when estimating the planetary ion escape rate in the magnetotail. In all, future comparative and more comprehensive studies on Venus, Mars, and Titan may help us discover more about the factors that may displace the structure of the induced magnetotail and improve our knowledge about the space environment of these unmagnetized planets.

Acknowledgments

The MAVEN data used for this study are publicly available from the NASA Planetary Data System (https://pds-ppi.igpp.ucla.edu/). Y. Z. Wen is supported by undergraduate research fellowship from Chinese Academy of Sciences. Z. J. Rong is funded by National Natural Science Foundation of China (Grant). The authors would like to thank the MAVEN team for the data and mission support.

References

1. Bertucci C, Duru F, Edberg N, Fraenz M, Martinecz C, Szego K, Vaisberg O. (2011). The

Induced Magnetospheres of Mars, Venus, and Titan. SPACE SCI REV, 162(1-4), 113-171. doi: 10.1007/s11214-011-9845-1

2. Connerney JEP, Espley J, Lawton P, Murphy S, Odom J, Oliversen R, Sheppard D. (2015). The MAVEN Magnetic Field Investigation. SPACE SCI REV, 195(1-4), 257-291. doi: 10.1007/s11214-015-0169-4

3. DiBraccio GA, Dann J, Espley JR, Gruesbeck JR, Soobiah Y, Connerney JEP, Halekas JS, Harada Y, Bowers CF, Brain DA, Ruhunusiri S, Hara T, Jakosky BM. (2017). MAVEN observations of tail current sheet flapping at Mars. Journal of Geophysical Research: Space Physics, 122(4), 4308-4324. doi: 10.1002/2016JA023488

4. DiBraccio GA, Espley JR, Gruesbeck JR, Connerney JEP, Brain DA, Halekas JS, Mitchell DL, McFadden JP, Harada Y, Livi R, Collinson G, Hara T, Mazelle C, Jakosky BM. (2015). Magnetotail dynamics at Mars: Initial MAVEN observations. GEOPHYS RES LETT, 42(21), 8828-8837. doi: https://doi.org/10.1002/2015GL065248

5. Dong C, Bougher SW, Ma Y, Toth G, Lee Y, Nagy AF, Tenishev V, Pawlowski DJ, Combi MR, Najib D. (2015). Solar wind interaction with the Martian upper atmosphere: Crustal field orientation, solar cycle, and seasonal variations. Journal of Geophysical Research: Space Physics, 120(9), 7857-7872. doi: https://doi.org/10.1002/2015JA020990

6. Dubinin E, Fraenz M. (2015). Magnetotails of Mars and Venus. Magnetotails in the solar system, 207, 34-59

7. Fang X, Liemohn MW, Nagy AF, Luhmann JG, Ma Y. (2010). On the effect of the martian crustal magnetic field on atmospheric erosion. ICARUS, 206(1), 130-138. doi: https://doi.org/10.1016/j.icarus.2009.01.012

8. Fang X, Liemohn MW, Nagy AF, Ma Y, De Zeeuw DL, Kozyra JU, Zurbuchen TH. (2008). Pickup oxygen ion velocity space and spatial distribution around Mars. Journal of Geophysical Research: Space Physics, 113(A2). doi: https://doi.org/10.1029/2007JA012736

9. Halekas JS, Brain DA, Lillis RJ, Fillingim MO, Mitchell DL, Lin RP. (2006). Current sheets at low altitudes in the Martian magnetotail. GEOPHYS RES LETT, 33(13). doi: 10.1029/2006GL026229

10. Halekas JS, Taylor ER, Dalton G, Johnson G, Curtis DW, McFadden JP, Mitchell DL, Lin RP, Jakosky BM. (2015). The Solar Wind Ion Analyzer for MAVEN. SPACE SCI REV, 195(1-4), 125-151. doi: 10.1007/s11214-013-0029-z

11. Harnett EM. (2005). Three-dimensional fluid simulations of plasma asymmetries in the Martian magnetotail caused by the magnetic anomalies. Journal of Geophysical Research, 110(A7). doi: 10.1029/2003JA010315
12. Jakosky BM, Lin RP, Grebowsky JM, Luhmann JG, Mitchell DF, Beutelschies G, Priser T, Acuna M, Andersson L, Baird D, Baker D, Bartlett R, Benna M, Bougher S, Brain D, Carson D, Cauffman S, Chamberlin P, Chaufray JY, Cheatom O, Clarke J, Connerney J, Cravens T, Curtis D, Delory G, Demcak S, DeWolfe A, Eparvier F, Ergun R, Eriksson A, Espley J, Fang X, Folta D, Fox J, Gomez-Rosa C, Habenicht S, Halekas J, Holsclaw G, Houghton M, Howard R, Jarosz M, Jedrich N, Johnson M, Kasprzak W, Kelley M, King T, Lankton M, Larson D, Leblanc F, Lefevre F, Lillis R, Mahaffy P, Mazelle C, McClintock W, McFadden J, Mitchell DL, Montmessin F, Morrissey J, Peterson W, Possel W, Sauvaud JA, Schneider N, Sidney W, Sparacino S, Stewart AIF, Tolson R, Toublanc D, Waters C, Woods T, Yelle R, Zurek R. (2015). The Mars Atmosphere and Volatile Evolution (MAVEN) Mission. SPACE SCI REV, 195(1-4), 3-48. doi: 10.1007/s11214-015-0139-x
13. Liemohn MW, Xu S, Dong C, Bougher SW, Johnson BC, Ilie R, De Zeeuw DL. (2017). Ionospheric control of the dawn‐dusk asymmetry of the Mars magnetotail current sheet. Journal of Geophysical Research: Space Physics, 122(6), 6397-6414. doi: 10.1002/2016JA023707
14. Luhmann JG, Dong C, Ma Y, Curry SM, Mitchell D, Espley J, Connerney J, Halekas J, Brain DA, Jakosky BM, Mazelle C. (2015). Implications of MAVEN Mars near-wake measurements and models. GEOPHYS RES LETT, 42(21), 9087-9094. doi: https://doi.org/10.1002/2015GL066122
15. Ma Y. (2002). Three-dimensional multispecies MHD studies of the solar wind interaction with Mars in the presence of crustal fields. Journal of Geophysical Research, 107(A10). doi: 10.1029/2002JA009293
16. Ma YJ, Nagy AF, Russell CT, Strangeway RJ, Wei HY, Toth G. (2013). A global multispecies single-fluid MHD study of the plasma interaction around Venus. Journal of Geophysical Research: Space Physics, 118(1), 321-330. doi: 10.1029/2012JA018265
17. McComas DJ, Spence HE, Russell CT, Saunders MA. (1986). The average magnetic field draping and consistent plasma properties of the Venus magnetotail. Journal of Geophysical Research, 91(A7), 7939. doi: 10.1029/JA091iA07p07939

18. McFadden JP, Kortmann O, Curtis D, Dalton G, Johnson G, Abiad R, Sterling R, Hatch K, Berg P, Tiu C, Gordon D, Heavner S, Robinson M, Marckwordt M, Lin R, Jakosky B. (2015). MAVEN SupraThermal and Thermal Ion Compostion (STATIC) Instrument. SPACE SCI REV, 195(1-4), 199-256. doi: 10.1007/s11214-015-0175-6

19. Mitchell DL, Mazelle C, Sauvaud JA, Thocaven JJ, Rouzaud J, Fedorov A, Rouger P, Toublanc D, Taylor E, Gordon D, Robinson M, Heavner S, Turin P, Diaz-Aguado M, Curtis DW, Lin RP, Jakosky BM. (2016). The MAVEN Solar Wind Electron Analyzer. SPACE SCI REV, 200(1-4), 495-528. doi: 10.1007/s11214-015-0232-1

20. Nagy AF, Winterhalter D, Sauer K, Cravens TE, Brecht S, Mazelle C, Crider D, Kallio E, Zakharov A, Dubinin E. (2004). The plasma environment of Mars. SPACE SCI REV, 111(1), 33-114

21. Romanelli N, Bertucci C, Gómez D, Mazelle C. (2015). Dependence of the location of the Martian magnetic lobes on the interplanetary magnetic field direction: Observations from Mars Global Surveyor. Journal of Geophysical Research: Space Physics, 120(9), 7737-7747. doi: 10.1002/2015JA021359

22.Romanelli N, Gómez D, Bertucci C, Delva M. (2014). STEADY-STATE MAGNETOHYDRODYNAMIC FLOW AROUND AN UNMAGNETIZED CONDUCTING SPHERE. The Astrophysical Journal, 789(1), 43. doi: 10.1088/0004-637X/789/1/43

23. Rong ZJ, Barabash S, Futaana Y, Stenberg G, Zhang TL, Wan WX, Wei Y, Wang XD, Chai LH, Zhong J. (2014). Morphology of magnetic field in near-Venus magnetotail: Venus express observations. Journal of Geophysical Research: Space Physics, 119(11), 8838-8847. doi: 10.1002/2014JA020461

24. Rong ZJ, Barabash S, Stenberg G, Futaana Y, Zhang TL, Wan WX, Wei Y, Wang XD. (2015). Technique for diagnosing the flapping motion of magnetotail current sheets based on single-point magnetic field analysis. Journal of Geophysical Research: Space Physics, 120(5), 3462-3474. doi: https://doi.org/10.1002/2014JA020973

25. Rong ZJ, Barabash S, Stenberg G, Futaana Y, Zhang TL, Wan WX, Wei Y, Wang XD, Chai LH, Zhong J. (2015). The flapping motion of the Venusian magnetotail: Venus Express observations. Journal of Geophysical Research: Space Physics, 120(7), 5593-5602. doi: https://doi.org/10.1002/2015JA021317

26. Rong ZJ, Stenberg G, Wei Y, Chai LH, Futaana Y, Barabash S, Wan WX, Shen C. (2016). Is

673 the flow-aligned component of IMF really able to impact the magnetic field structure of
674 Venusian magnetotail? Journal of Geophysical Research: Space Physics, 121(11), 10, 910-978,
675 993. doi: 10.1002/2016JA022413
676 27. Simon S, Motschmann U. (2009). Titan's induced magnetosphere under non-ideal upstream
677 conditions: 3D multi-species hybrid simulations. PLANET SPACE SCI, 57(14-15), 2001-2015.
678 doi: 10.1016/j.pss.2009.08.010
679 28. Simon S, van Treeck SC, Wennmacher A, Saur J, Neubauer FM, Bertucci CL, Dougherty MK.
680 (2013). Structure of Titan's induced magnetosphere under varying background magnetic field
681 conditions: Survey of Cassini magnetometer data from flybys TA-T85. Journal of Geophysical
682 Research: Space Physics, 118(4), 1679-1699. doi: 10.1002/jgra.50096
683 29. Sonnerup BU, Scheible M. (1998). Minimum and maximum variance analysis. Analysis
684 methods for multi-spacecraft data, 1, 185-220
685 30. Vignes D, Mazelle C, Rme H, Acuña MH, Connerney JEP, Lin RP, Mitchell DL, Cloutier P,
686 Crider DH, Ness NF. (2000). The solar wind interaction with Mars: Locations and shapes of
687 the bow shock and the magnetic pile-up boundary from the observations of the MAG/ER
688 Experiment onboard Mars Global Surveyor. GEOPHYS RES LETT, 27(1), 49-52. doi:
689 10.1029/1999GL010703
690 31. Zhang TL, Du J, Ma YJ, Lammer H, Baumjohann W, Wang C, Russell CT. (2009).
691 Disappearing induced magnetosphere at Venus: Implications for close-in exoplanets.
692 GEOPHYS RES LETT, 36(20). doi: 10.1029/2009GL040515
693